Nature of AGN Feedback: Testing Numerical Models with Chandra Observations

Corey Brummel-Smith,[1] Yuan Li,[2] Daisuke Nagai[3] Irina Zhuravleva[4]
[1] *Center for Relativistic Astrophysics, Georgia Institute of Technology, Atlanta, GA, 30332, USA*
[2] *Center for Computational Astrophysics (CCA), New York, NY, USA*
[3] *Department of Physics, Yale University, New Haven, CT 06520, USA*
[4] *Kavli Institute for Particle Astrophysics and Cosmology, Stanford University, 452 Lomita Mall, Stanford, California 94305-4085, USA*

18 October 2018

ABSTRACT
Analysis of the observed X-ray emission from the cores of galaxy clusters has proven to be a novel way of probing how outflows from active galactic nuclei (AGN) perturb the intracluster medium (ICM). AGN outflows disrupt their environment in a variety of ways. They can generate shocks, turbulence, and mix different phases of the gas in the ICM. Cosmic ray feedback from an AGN is also capable of inflating hot, energetic, cosmic ray bubbles. This shows that AGN are important for understanding cluster evolution. However, we do not yet know if our numerical AGN feedback models can reproduce all the observed features we see in the X-ray emission from observed clusters. In this paper, we present a comparison of mock X-ray observations of a simulated galaxy cluster with Chandra X-ray images of the cluster Abell 2052. By performing the same analysis on the mock images and the real ones, we are able to directly compare the simulation with observations, and test the effectiveness of the momentum-driven AGN feedback model. We find that the central 20 kpc of the simulated cluster core is dominated by isobaric perturbations, consistent with what is seen in A2052, while the outer 20-100 kpc show more adiabatic perturbations, which is not seen in A2052. Overall, the simulation shows slightly stronger emissivity fluctuations than A2052.

1 INTRODUCTION

It is well known that simulations of cool core galaxy clusters develop a strong cooling flow in the absence of any feedback mechanisms. In this process, X-ray emission from the ICM rapidly cools the gas and it condenses to form stars. In this scenario, the observed star formation rates can be as large as hundreds to even $1000 M_{\odot} yr^{-1}$ (Fabian 1994). This is much larger than ever seen in nature (McNamara & O'Connell 1989; O'Dea et al. 2008).

One possible solution to this classical cooling flow problem is AGN feedback. Accretion of cold gas onto a supermassive black hole, drives outflows of hot gas with sufficient energy to heat the ICM and suppress the cooling flow. It has been shown by numerous authors that there are a variety of methods by which the AGN can heat the environment. Namely via shocks, turbulence, and mixing of the hot and cold gas. Of course, these feedback mechanisms do not uniformly heat the ICM, they all cause different fluctuations in the temperature, density, and pressure of the gas. This poses a couple important questions; what are the dominant types of perturbations caused by the AGN, and how can we determine the nature of these perturbations? The first question is addressed in the Section 5 and the second is addressed in Section 2.

To understand how AGN affect their environment, it is necessary to understand the nature of how they perturb the ICM. This requires an understanding of the density and temperature fluctuations and the effective equation of state (EOS) for the gas perturbations (described in 2). The observational challenge is, density and temperature are not directly observable. All that observers have to work with is the light gathered by telescopes. Luckily, nature has encoded information about the density and temperature into X-ray emission from the gas. Any fluctuations in the density and temperature cause corresponding fluctuations in the X-ray emission from the gas. This we can measure with an X-ray telescope such as Chandra. By directly observing fluctuations in the X-ray emissivity, we are able to indirectly measure fluctuations in the density and temperature.

The goal of this study is to use fluctuations in the X-ray emissivity to measure the effective EOS in different regions of the ICM, and hence determine what types of perturbations are present in both simulated and real cluster cores. The method used in this research has previously been used to analyze Chandra X-ray images of real galaxy clusters (see Zhuravleva et al. 2016, 2017). However, this method has never been used to perform the same analysis on mock X-ray images of simulated clusters, and that is what we focus on in this work. In particular, we perform the X-ray fluctuation analysis on a snapshot that has similar features to the cluster Abell 2052 (A2052) and directly compare the X-ray emission from these clusters. This is the first time that we have a direct comparison of the X-ray emissivity fluctuations in both simulations and observations. Not only does this allow us to test the AGN feedback model used in the simulation to verify if it can reproduce the observational signatures of real clusters, but we can also use these mock X-ray observations to test any observational biases in the X-ray emissivity fluctuation analysis. This can help reveal the effectiveness of the method and allow for better interpretation of observational data. We also do a more qualitative, visual comparison of our mock Chandra images with real Chandra images of observed clusters. We show that our idealized simulation is able to generate clusters that look qualitatively similar to real ones, namely the Perseus and Centaurus clusters.

2 METHODS

Here we describe the method of analyzing X-ray emissivity fluctuations to determine the nature of perturbations in density and temperature caused by the AGN outflows. Much of this is described in (Zhuravleva et al. 2016) but we present it here for clarity and completeness since it is directly related to how we perform our analysis.

Different types of perturbations are characterized by different effective equations of state (EOS). Here an EOS refers to a functional relationship between the density and temperature of the gas. There are many different types of density and temperature fluctuations in nature, all characterized by a different EOS. Typically an EOS is modeled as a polytrope, $T \propto n^{\eta}$ where, T is the temperature, n is the number density, and $\eta = \gamma - 1$ is related to the adiabatic index, γ, which characterizes the type of perturbation. The three types of perturbations considered here are adiabatic ($\eta = 2/3$), isobaric ($\eta = -1$), and isothermal ($\eta = 0$). Each of these different EOS describe a different physical process. Examples of adiabatic perturbations would be sound waves or weak shocks, as long as the entropy of the gas is unchanged, the mach number is low, and there is not heat exchange with the environment. Isobaric perturbations could be seen in the case of slow displacements of the gas, more specifically, slower than the local sound speed. Isobaric perturbations could also occur in regions where there is strong cooling where the sound crossing time is small, such as in the central region of the simulated cluster. Isothermal perturbations occur when there are changes in the density at constant temperature. In astrophysics contexts related to AGN, this can occur in bubbles inflated by AGN outflows (Zhuravleva et al. 2015).

From the polytropic EOS, one can do a first order expansion in T and n about their mean values to show that the fractional fluctuations in temperature are linearly dependent on the fractional density fluctuations.

$$\frac{\delta T}{T} = \eta \frac{\delta n}{n} \tag{1}$$

The emissivity f, is related to the density and cooling function through

$$f \propto n^2 \Lambda(T) \tag{2}$$

The ICM cools due to this X-ray emission, and emits X-rays of different energies. The cooling function, $\Lambda(T)$, is different for gas emitting X-rays in different energy bands and hence, fluctuations in temperature will cause different fluctuations in the X-ray emission in different energy bands. This is shown in Figure 1. Essentially, different energy bands respond differently to changes in temperature. It is this fact that enables one to compute the EOS from measurements of emissivity fluctuations. First we assume the density, temperature, and emissivity fluctuations can be decomposed as a sum of fluctuations of each different type.

$$\frac{\delta x}{x} = \sum_i \left(\frac{\delta x}{x}\right)_i \tag{3}$$

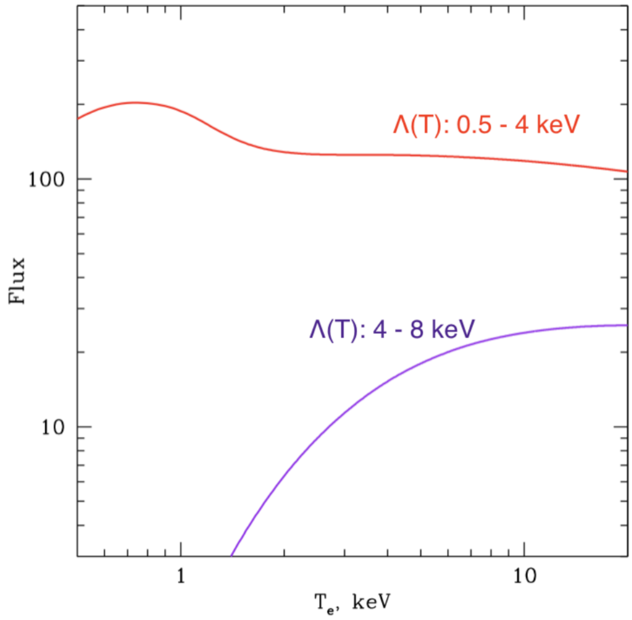

Figure 1. X-ray emissivity flux in two different energy bands as a function of temperature. Red: soft band (0.5 - 4 keV), Purple: hard band (4 - 8 keV). Figure from Zhuravleva et al. (2015)

where $x \in \{T, n, f\}$ and $i \in \{\text{adiabatic, isobaric, isothermal}\}$. Using equations 1, 2, 3 we can solve for $(\delta f/f)_i$

$$\left(\frac{\delta f}{f}\right)_i = \left(\frac{\delta n}{n}\right)_i \left[2 + \eta_i \frac{d \ln \Lambda(T)}{d \ln T}\right] \tag{4}$$

Notice if we take the ratio of emissivity fluctuations in two different energy bands, hard and soft, we get an equation that is independent of the density fluctuations, and is a just a function of the cooling in both bands and the adiabatic index η.

$$\frac{(\delta f_h/f_h)_i}{(\delta f_s/f_s)_i} = \frac{2 + \eta_i \frac{d \ln \Lambda_h(T)}{d \ln T}}{2 + \eta_i \frac{d \ln \Lambda_s(T)}{d \ln T}} \tag{5}$$

Given that we know the cooling functions in both energy bands, the only free parameter is η. One can see that for $\eta = 0$ – corresponding to isothermal perturbations – the ratio equals one. Similarly for $\eta = 2/3$ or $\eta = -1$, the ratio will be either greater than or less than one for adiabatic or isobaric perturbations, respectively. Thus, by measuring the sign of the ratio of the emissivity fluctuations in two different bands, we are able to determine the dominant type of perturbation and the effective EOS.

2.1 Power Spectra via Mexican Hat Filter

In practice, we measure the the emissivity fluctuations by analyzing the pixel brightness in X-rayimages, either real, or mock (described in section 4). We can do more than just look at the ratio of the emissivity fluctuations though. By calculating the power spectra of the emissivity fluctuations we are able to probe the nature of perturbations on different length scales. Just like with the emissivity fluctuations themselves, we can determine the nature of perturbations from the power spectra of the fluctuations. These relations for the three types of perturbations are shown below, where P_{hard} and

$P_{\rm soft}$ are the power spectra of the fluctuations in the hard and soft bands respectively.

- Adiabatic: $P_{\rm hard} > P_{\rm soft}$
- Isothermal: $P_{\rm hard} \approx P_{\rm soft}$
- Isobaric: $P_{\rm hard} < P_{\rm soft}$

It is often beneficial to look at the power spectra in certain regions of the simulations to investigate the fluctuations in different environments such as in bubbles, in shocked regions, and in the center of the AGN. This requires masking out portions of the image which makes it nontrivial to calculate the power spectra. Masking out regions of the image introduces hard edges which pose problems for calculating the power spectra using the standard two-dimensional Fourier transform method. In order to handle this problem we use a different method of calculating the power spectrum. We use a Mexican Hat filter to filter out fluctuations at a given length scale. The power at that length scale is then computed from the variance of the filtered fluctuations. The details of this method are explained in Arévalo et al. (2012). Here we present a brief overview of the method here.

The kernel for the Mexican-Hat filter is the difference of two Gaussian kernels with slightly different widths. The widths of the Gaussians are related to the length scale at which the emissivity fluctuations are filtered out at. The Mexican-Hat filter $\mathcal{F}_k$, for a given length scale k, is defined as follows. We define $k \equiv 1/x$ without the usual factor of 2π.

$$\mathcal{F}_k(x) = G_{\sigma_-}(x) - G_{\sigma_+}(x) \tag{6}$$

$$\sigma_\pm = \sigma\,(1+\epsilon)^{\pm 1/2} \tag{7}$$

$$\sigma = \frac{1}{\sqrt{2\pi^2}}\frac{1}{k} \tag{8}$$

$$G_\sigma(x) = \frac{1}{\sqrt{2\pi\sigma^2}}\exp\left(\frac{-x^2}{2\sigma^2}\right) \tag{9}$$

where ϵ in equation 7 is a small number. We use $\epsilon = 10^{-3}$. Before applying the filter, we must mask out the whole image except for the region of interest. Call this region R. The mask M, is an array the same shape as the original image I, with the value 1 for all pixels $\in$ R, and zero everywhere else. The new image S_k, with fluctuations filtered out at length scale k is given by

$$S_k = \left(\frac{G_{\sigma_-} * I}{G_{\sigma_-} * M} - \frac{G_{\sigma_+} * I}{G_{\sigma_+} * M}\right) M \tag{10}$$

where $*$ is the convolution operator. The power P_k, at wavenumber k, is related to the variance of the filtered image V_k.

$$V_k = \frac{N_{\rm total}}{N_{\rm mask}}\sum S_k^2 \tag{11}$$

$$P_k = \frac{V_k}{\pi\epsilon^2 k^2} \tag{12}$$

where $N_{\rm total}$ is the total number of pixels in the image, and $N_{\rm mask}$ is the number of pixels in the region of interest. Equation 12 is specific to the two dimensional case, but this method can be extended to n dimensions (Arévalo et al. 2012).

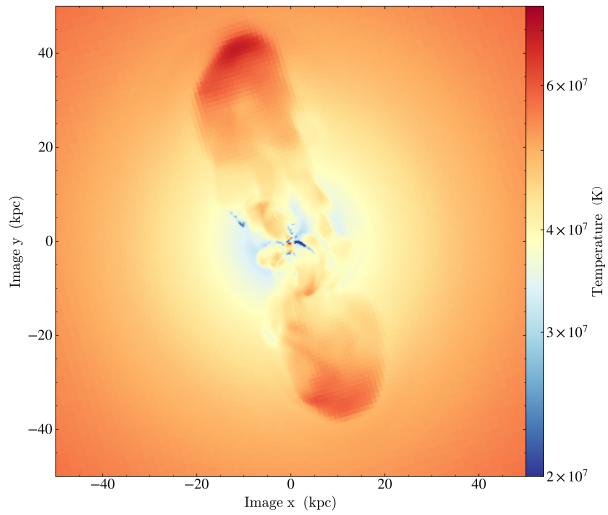

Figure 2. This is a density-weighted temperature projection showing the AGN outflows from the SMBH at the center of the simulation box. The vertical extent of the image is approximately 100 kpc. Note: because this is a density weighted projection, the values on the colorbar do not reflect the actual range of temperatures in the cluster core. Image generated with yt (Turk et al. 2011).

3 SIMULATIONS

A detailed description of the simulation we analyze is described in Li & Bryan (2012) and Li & Bryan (2014). Here we just state some basic details. The cool-core galaxy cluster simulation is designed specifically to study the effects of the AGN feedback on the ICM. It was run with the adaptive mesh refinement code for magneto-hydrodynamics, Enzo (Bryan et al. 2014), although this simulation does not include magnetic fields. The simulation is idealized in the sense that it is a single, isolated, cluster in a non cosmological box. This simplifies the problem because there is no interaction with other clusters and no individual galaxies or merger events. This allows us to focus specifically on the effects of the AGN outflows themselves. Figure 2 shows an image of the outflows. It is a 16 Mpc^3 box with a $3 \times 10^8 M_\odot$ super-massive black hole (SMBH) at the center. Accretion of cool gas onto the SMBH drives outflows which feed energy and momentum back into the ICM. It uses a sub-grid, momentum-driven feedback model which has been show to be effective at offsetting the radiative cooling problem (Li et al. 2015).

4 MOCK X-RAY IMAGES

To perform our analysis, we need mock images of the simulated galaxy cluster. To generate the mock Chandra X-ray images, we use the Python package, pyXSIM (ZuHone & Hallman 2016). We create our mock images as if the simulated cluster were at the physical location of the Perseus cluster and observed by the Chandra X-ray observatory for the same duration as when Chandra imaged Perseus. This means our simulated cluster is placed at redshift z = 0.0179 at (RA, Dec) = (3h 18m 0s, 41.5°) on the sky. Using pyXSIM, we generate X-ray photons with energies ranging from 0.5 - 3.5 keV (soft band) and 3.5 - 7.5 keV (hard band) for each cell in the simulation. The photons are then projected along the line of sight to a simulated Chandra telescope. These photons are convolved with a Chandra ACIS-I instrument response model giving a realistic image similar to what one would obtain from real observations. The photons are gathered for 270 hrs in a collecting area of 0.04 m^2, with a field of view of 0.0394 degrees. We have made images with different exposure times of 27 hrs and 2.7 hrs, and images from different viewing angles but have not analyzed those yet. To simplify the analysis we have not artificially included any point sources in the photon production step. In practice, such point sources, when present, are often removed from the data before performing the fluctuation analysis. By not including them we can skip this step. We do however, include the "tbabs" foreground ISM absorption model with an assumed n_H column density of $0.04 \times 10^{22}\ cm^{-2}$.

We generated mock images for many different snapshots. From an observational standpoint, mock images of different simulation snapshots are just like different clusters since each snapshot shows the cluster at a different stage in its evolution. Therefore, with just one simulation, we can generate a whole suite of mock X-ray cluster images. We then looked through the set of mock images and found some that look similar to well known observed clusters. In particular we have identified two mock X-ray images of the simulated cluster core that look similar to the cores of the Perseus and Centaurus clusters. In Figure 3, we show comparisons of our mock Chandra images and real Chandra images of these clusters. One can see that our mock images show some of the same features as the real ones and visually look somewhat similar to their observational counterparts. In the bottom panel of Figure 3, one can see that both Centaurus and the simulated cluster show a somewhat spherical shape with a bright central region and decreasing intensity at larger radii. In the top panel of Figure 3, one can see that both Perseus and the simulated cluster have bubble-like features as well as regions that appear to be shocks. X-ray analysis of Perseus shows that, in fact, there are shocked regions present in this image (Zhuravleva et al. 2016). This shows that at least qualitatively, we are able to create somewhat realistic clusters with our simplified AGN feedback simulation. It is interesting to note that the mock Chandra image similar to Perseus has the line of sight down the axis of the bubble, perpendicular to the plane of the jets. This could be an indication that we are observing Perseus "head-on", with our line of sight along outflows from the AGN.

To properly test the simulation's AGN feedback model in a more quantitative manner, we perform the fluctuation analysis and compare the nature of perturbations in the simulation and observations. We perform the X-ray fluctuation analysis described in section 2 on the simulation to determine the effective EOS, and compare with the results obtained from Chandra X-ray images of the real cluster, Abell 2052. This is an ideal cluster to compare with because it has a similar star formation rate as the particular snapshot of the simulation analyzed in this paper. The observed star formation rate in A2052 is approximately $0.6 M_{\odot} yr^{-1}$ (Blanton et al. 2003), while the star formation rate of the simulated cluster is approximately $0.2 M_{\odot} yr^{-1}$ at the time of the mock observation. A2052 also shows similar features as the snapshot presented here, namely they both have bubbles/cavities of low density gas and shocked regions, as well as a bright central region in the cluster core. In this paper, we only perform the fluctuation analysis on the this one snapshot. In the future we will also perform the fluctuation analysis on the snapshots that resemble Perseus and Centaurus.

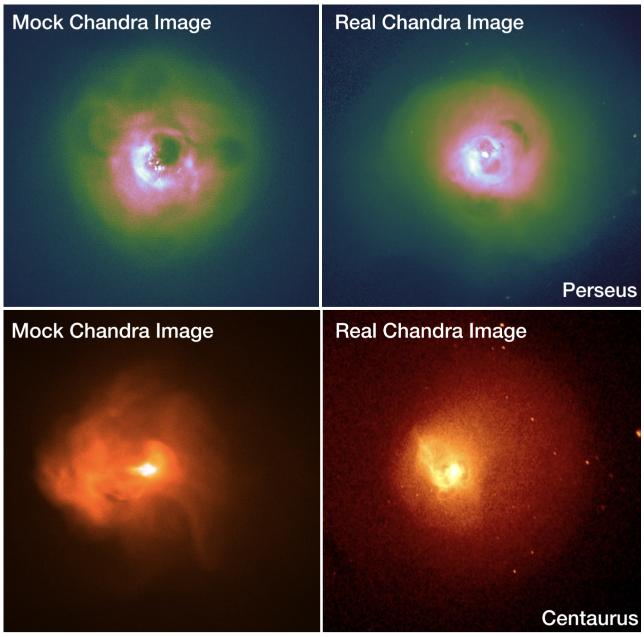

Figure 3. Top Left: Mock X-ray image of the simulated cluster core with the line of sight down one of the outflows. Top Right: Chandra X-ray image of the Perseus cluster core (NASA/CXC/IoA/A.Fabian et al). Bottom Left: Another mock image of the simulated cluster at a different point in time. Bottom Right: Chandra image of the Centaurus cluster core (Sanders et al. 2016)

5 RESULTS

For the results presented here, we analyze mock X-ray images, in the hard and soft bands, of our simulated cluster during a stage in its evolution where it is actively accreting gas onto the SMBH. This produces prominent bipolar outflows which generate weak shocks on the edges of the outflowing bubbles and elsewhere in the cluster core. We compare the hard and soft band residual images with those of a real cluster, Abell 2052, imaged by Chandra. These images are shown in Figure 4. While these two clusters do not look morphologically similar, they were originally chosen for comparison because of their similar star formation rates.

First we measure radial profiles of fluctuations in the surface brightness. The fluctuations are measured relative to a global profile, a so-called, β-model. The β-model (Equation 13) is similar to a power-law with exponent β:

$$I = I_0 \left(1 + \left(\frac{r}{r_0}\right)^2\right)^{-\beta} \quad (13)$$

Here, r_0 is the core radius and I_0 is the surface brightness at the center of the core. These models are often used in cluster astrophysics to characterize the global trend of quantities such as density, temperature, and X-ray emissivity, in a spherically averaged sense – or angularly averaged for 2D data. In Figure 5, it can be seen that the radial profiles in both the hard and soft bands for both the simulated and observed data show similar behavior. They both exhibit a bump at the peak of their brightness and then decline at larger radii with a power law tail. These surface brightness profiles show that there is some consistency between our simulated cluster and A2052, even though they do not look morphologically similar.

A better comparison, and insight into the physical nature of

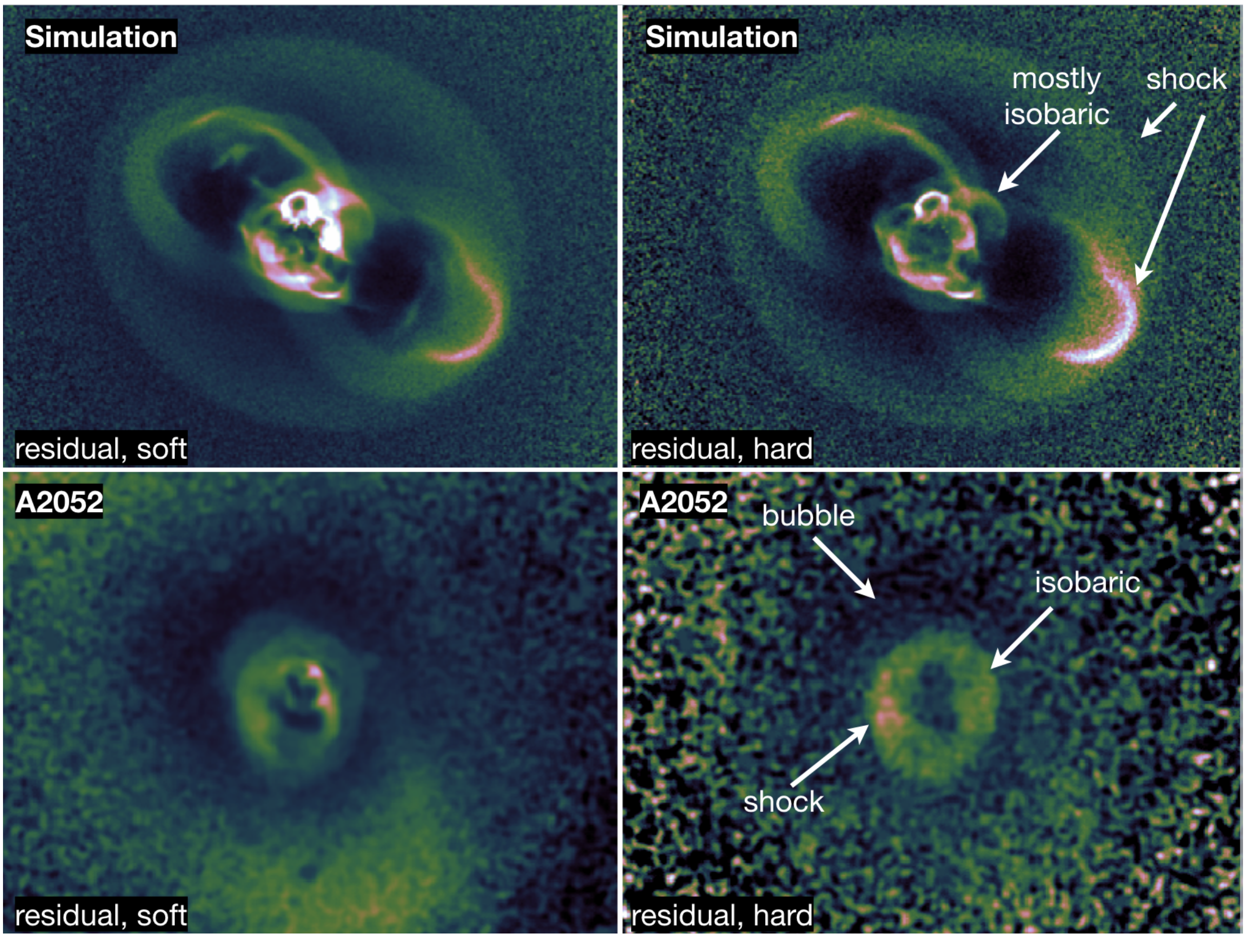

Figure 4. Residual X-ray images showing fluctuations in the X-ray emission in both the simulated cluster and A2052 in two different energy bands. Top row: mock Chandra images. Bottom row: real Chandra images. Left column: soft X-rays (0.5 - 3.5 keV). Right column: hard X-rays (3.5 - 7.5 keV).

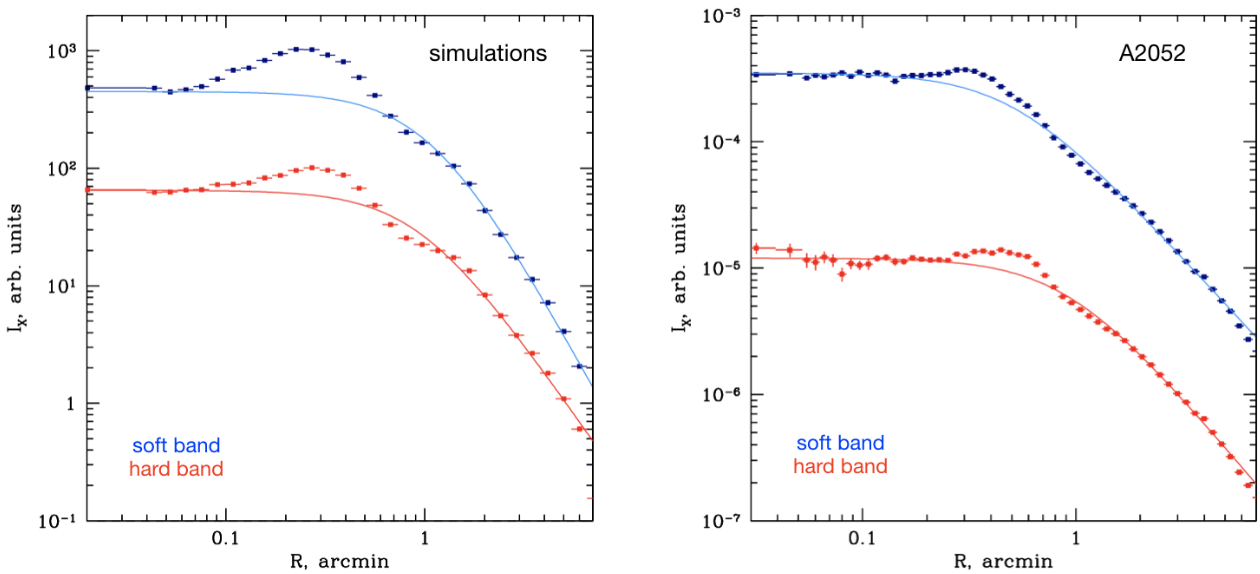

Figure 5. Surface brightness radial profiles from residual images of X-rayemission from the simulated cluster (left) and A2052 (right). The points are the values from the data. Solid lines are beta models fitted to the data. Soft X-rays (0.5-3.5 keV) are in blue. Hard X-rays (3.5-7.5 keV) are in red.

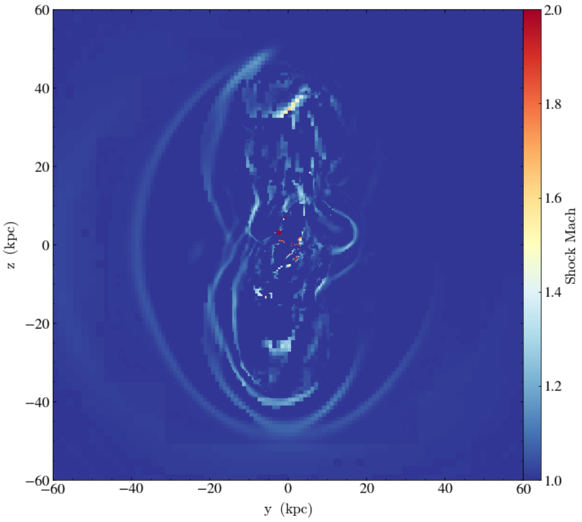

Figure 6. This shows a slice plot through the center of the core of the simulated cluster where the color shows the Mach number of the shocked gas. Un-shocked regions are shown in dark blue with a shock Mach number of 1.0.

these clusters comes from examination of the power spectra. In Figure 7, we plot the 2D power spectra for the emissivity fluctuations calculated in various regions in the residual images of the simulated cluster core. First, in Figure 7a, we show the power spectra in the central region of the core ∼20 kpc across (0.5 arcmin). There is more power in the soft band than the hard band at all length scales, suggesting this region is likely dominated by isobaric perturbations. This is somewhat consistent with A2052, however. A2052 also shows isothermal perturbations in the inner 24-35 kpc. There is an interesting difference between the simulation and observation. The simulation shows more power at all length scales, in both bands than in A2052. From the mock images we find $A_k \gtrapprox 1$ for both the hard and soft bands, while A2052 has $A_k < 1$ (soft) and $A_k < 0.5$ (hard) (Zhuravleva et al. 2017). Next, we examine an ∼20 kpc region near the edge of the lower bubble. As seen in a map of the shock mach number (Figure 6), the edge of the bubble is a weakly shocked region with mach number $\mathcal{M} \approx 1.2$. For a region dominated by a weak shock, we would expect to see this region dominated by adiabatic perturbations, and hence see more power in the hard band than the soft. Figure 7b shows just that. There is more power in the hard band than the soft band for all wave numbers. We have not yet analyzed a shocked region in A2052.

It is interesting to look at the power spectra in the central 100 kpc (2.5 arcmin) of the simulated cluster core. Figure 7c shows that this region encompasses the full extent of the AGN jets. We find roughly equal power in the hard band and the soft for large wave numbers between 0.01 and 0.02 arcsec. This is characteristic of isothermal perturbations. While at smaller scales, the fluctuations are more isobaric. This is consistent with what is seen in A2052 which exhibits isothermal fluctuations on large scales and isobaric on small scales. It is useful to analyze the cluster core with the bright central region removed because since this region is so bright, it can dominate the signal in the power spectra and make it difficult to properly interpret the data and infer the nature of perturbations. For this reason, we analyze the same 100 kpc region but with the inner 20 kpc removed. When we do this, we find the fluctuations are primarily adiabatic whereas in A2052, a similar region is mostly isobaric.

To summarize, the central region of the simulated cluster core is isobaric – more power in the soft band than the hard. The outer region with the center removed is adiabatic – more power in the hard band than the soft. But when we look at both of these regions together, it looks isothermal – equal power in the hard and soft bands. It appears what is happening is a cancellation effect. Power from inner isobaric region and outer adiabatic region add together giving equal power in both bands, even though the underlying fluctuations are probably not isothermal.

6 CONCLUSIONS

In conclusion, measuring the power spectra of X-ray emissivity fluctuations provides a novel method of testing AGN feedback models. While this method has been previously used to analyze Chandra observations and probe the nature of perturbations in real clusters, this is the first time it has been applied to mock Chandra images of simulated clusters. Here we have presented a direct comparison between the emissivity fluctuations in our simulated cluster and Abell 2052. We find that the nature of perturbations in our simulated cluster are primarily isobaric within the central 20 kpc and adiabatic in the 20-100 kpc region. This is consistent with observations of A2052 in the center, but not in the outer region. The inconsistency between the simulation and A2052 in the outer 20-100 kpc could be explained if the simulation has more shocks than A2052 does, but we do not know for sure if this is the case. More investigation is needed to properly explain this discrepancy. Also we find the emissivity fluctuations are stronger in the simulation than in observations of A2052. Since we have only compared the simulation with one observational sample, we cannot say whether or not the simulation has stronger shocks than real clusters on average and it is too soon to make a conclusion about the validity of AGN feedback model based on this discrepancy. Although we have only described the comparison between one snapshot from the simulation and one observational sample, we have generated many more mock Chandra images of the cluster at various stages in its evolution and will soon compare them with more observed clusters. We have also compared Chandra X-ray images of Perseus and Centaurus with X-ray images of the simulation at different stages in its evolution. We find that qualitatively, the simulated clusters share similar features with their observational counterparts. This shows the simulation is capable of reproducing realistic looking clusters.

7 FUTURE WORK

This project is still a work in progress, and we have a number of future tests to do before publication. First, we are going to test if there are observational biases that could affect the effective EOS inferred from the emmisivity fluctuation method. One observational bias we will investigate is the variation in the X-ray fluctuations due to viewing a cluster along different lines of sight. This can easily be done by analyzing mock X-ray images of the same simulated cluster from different viewing angles. This will give a measure of the robustness of the emissivity fluctuation method. For instance, if we look at at a specific region, such as a shock, from different viewing angles and get the same results, we can be confident that this method is capable of revealing the effective EOS, independent of the line of sight through the cluster. However, if we find the nature of

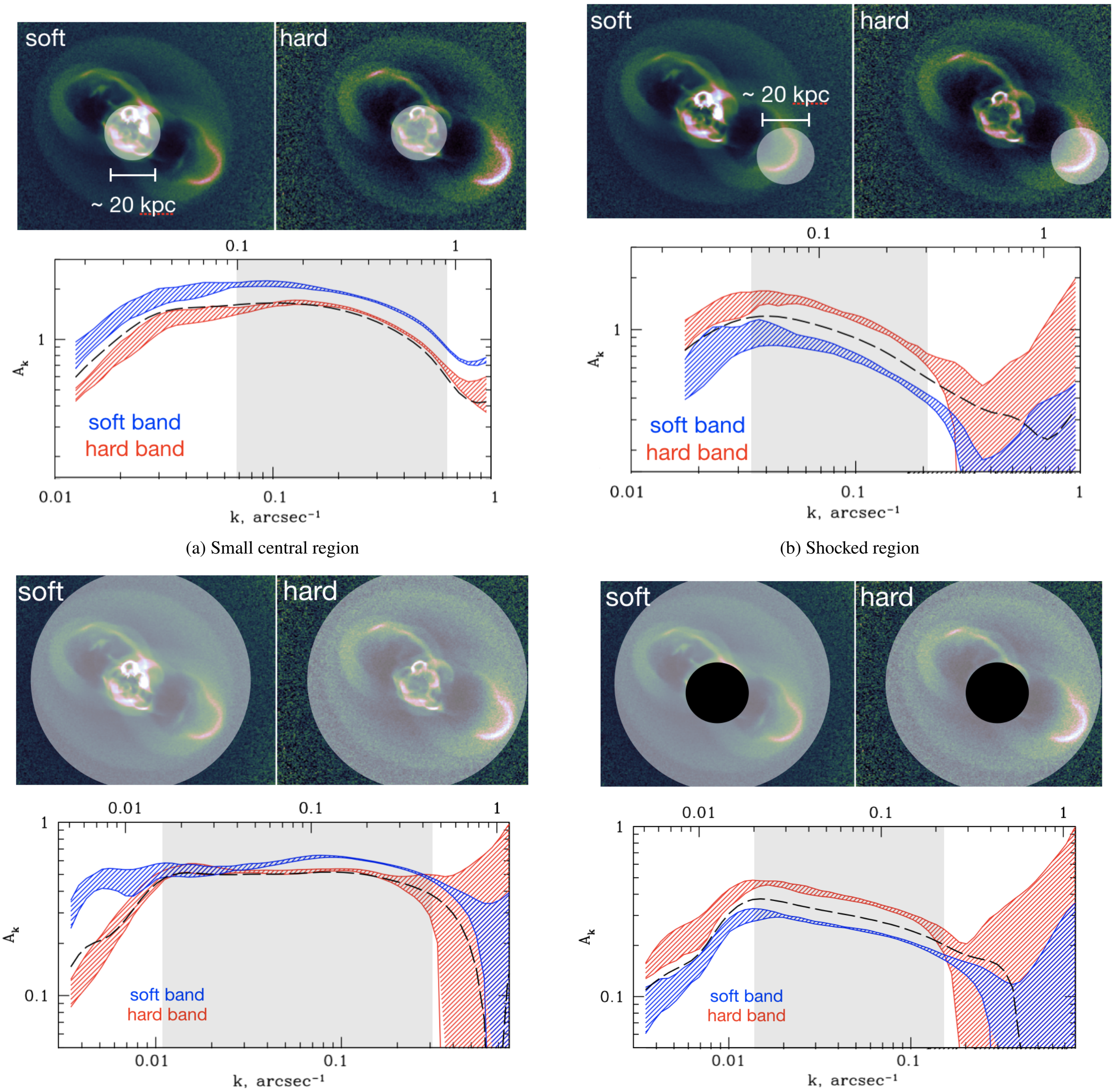

(a) Small central region

(b) Shocked region

(c) Full core with bright central region

(d) Full core without bright central region

Figure 7. For each of (a), (b), (c) and (d), the top panel shows residual mock Chandra images of the simulated cluster for both hard and soft X-rays with the region of interest highlighted. The bottom panel shows the emissivity fluctuation power spectra in both the hard (red) and blue (soft) X-rays.

perturbations has a strong dependence on viewing angle, then there must be significant projection effects that influence the measurement of the nature of perturbations. To further investigate these possible projection effects, we will do a more direct analysis of the effective EOS from the full 3-dimensional density and temperature fields in the simulation. One way this can be done is by fitting a polytropic EOS to a phase plot of the density and temperature fields. This will provide a direct measure of the adiabatic index and the nature of perturbations. We can then compare these results with those obtained from analysis of the mock images and determine if the EOS measured from the 3-dimensional data is consistent with the EOS inferred from the 2-dimensional X-ray images.

A second observational effect that could influence the measurement of the nature of perturbations is the exposure time of the images. Real telescope time is expensive, so we often cannot image the same cluster with different exposures. Simulated telescope time for our mock observations is very cheap since each observation takes only minutes to run on a computer, so we are able to image the same cluster with a wide range of exposure times varying many orders of magnitude. This way we can learn how the nature of perturbations changes as a function exposure time. One potential benefit that could come from this analysis would be finding a minimum exposure time for a given uncertainty in the X-ray fluctuation powerspectra. In this way, we might be able to help inform observers of how long they need to observe a cluster to get sufficiently reliable measurements.

Lastly, we are going to analyze more of the mock Chandra images of the simulated cluster at different times in its evolution. This will show how the effective EOS changes in different regions of the cluster over time. We will then find more observational counterparts that look similar to the simulated clusters, and compare the nature of perturbations in both. With more samples, and more comparisons, we will further test the momentum-driven AGN feedback model, and be able to make claims about its validity with a higher degree of certainty.

ACKNOWLEDGEMENTS

This work was initiated as a project for the Kavli Summer Program in Astrophysics held at the Center for Computational Astrophysics of the Flatiron Institute in 2018. The program was co-funded by the Kavli Foundation and the Simons Foundation. We thank them for their generous support. Also thank you to all the students, mentors, and staff, especially Greg Brian, Rachel Somerville, and Shatevia Wilkins.

REFERENCES

Arévalo P., Churazov E., Zhuravleva I., Hernández-Monteagudo C., Revnivtsev M., 2012, MNRAS, 426, 1793
Blanton E. L., Sarazin C. L., McNamara B. R., 2003, ApJ, 585, 227
Bryan G. L., et al., 2014, ApJS, 211, 19
Fabian A. C., 1994, ARA&A, 32, 277
Li Y., Bryan G. L., 2012, ApJ, 747, 26
Li Y., Bryan G. L., 2014, ApJ, 789, 153
Li Y., Bryan G. L., Ruszkowski M., Voit G. M., O'Shea B. W., Donahue M., 2015, ApJ, 811, 73
McNamara B. R., O'Connell R. W., 1989, AJ, 98, 2018
O'Dea C. P., et al., 2008, ApJ, 681, 1035
Sanders J. S., et al., 2016, MNRAS, 457, 82
Turk M. J., Smith B. D., Oishi J. S., Skory S., Skillman S. W., Abel T., Norman M. L., 2011, ApJS, 192, 9
Zhuravleva I., et al., 2015, in X-Ray Vision Workshop: Probing the Universe in Depth and Detail with the X-Ray Surveyor (X-Ray Vision Workshop), National Museum of the American Indian, Washington, DC, USA, 6-8 October 2015, article id.14. p. 14, doi:10.5281/zenodo.47420
Zhuravleva I., et al., 2016, MNRAS, 458, 2902
Zhuravleva I., Allen S. W., Mantz A. B., Werner N., 2017, preprint, (arXiv:1707.02304)
ZuHone J. A., Hallman E. J., 2016, pyXSIM: Synthetic X-ray observations generator, Astrophysics Source Code Library (ascl:1608.002)

This paper has been typeset from a TEX/LATEX file prepared by the author.